Paper-Like Writable Nanoparticle Network Sheets for Mask-Less MOF Patterning

Renheng Bo[#,], Mahdiar Taheri[#], Hongjun Chen, Jonathan Bradford, Nunzio Motta, Sachin Surve, Thanh Tran-Phu, Puneet Garg, Takuya Tsuzuki, Paolo Falcaro and Antonio Tricoli**

Dr. R. Bo, Dr. Hongjun Chen, Dr. Thanh Tran-Phu, Puneet Garg, Prof. Antonio Tricoli
Nanotechnology Research Laboratory, Research School of Chemistry, Australian National University, Canberra 2601, Australia

Dr. R. Bo
Applied Mechanics Laboratory (AML)
Department of Engineering Mechanics, Tsinghua University, Beijing 100084, People's Republic of China
Center for Flexible Electronics Technology, Tsinghua University, Beijing 100084, People's Republic of China

Dr. M. Taheri, Prof. T. Tsuzuki
Laboratory of Advanced Nanomaterials for Sustainability, Research School of Engineering, Australian National University, Canberra 2601, ACT, Australia

Dr. Hongjun Chen
School of Physics and The University of Sydney Nano Institute, The University of Sydney, Sydney, NSW, 2006 Australia

Dr. J. Bradford, Prof. N. Motta
Surface Science and 2D materials group, CPME School and Institute for Future Environments, Queensland University of Technology, Brisbane 4001, QLD, Australia

Dr. Sachin Surve
Solar PV Group, Research School of Electrical, Energy, and Materials Engineering, Australian National University, Canberra 2601, Australia

Prof. P. Falcaro
Institute of Physical and Theoretical Chemistry, Graz University of Technology, Stremayrgasse 9/Z2, 2010 Graz, Austria

Prof. Antonio Tricoli
Nanotechnology Research Laboratory, Faculty of Engineering University of Sydney, NSW 2006, Australia

[#]R. Bo and M. Taheri contributed equally to this work.

*Corresponding authors: antonio.tricoli@sydney.edu.au; renhengbo@mail.tsinghua.edu.cn

Abstract: Geometrical structuring of monolithic metal-organic frameworks (MOFs) components is required for their practical implementation in many areas, including electronic devices, gas storage/separation, catalysis, energy storage as well as bio-medical applications. Despite progress in structuring MOFs, an approach for the precise patterning of MOFs functional geometries such as channels, wells and membranes in the millimeter- to micro-meter depth is lacking. Here, we report a facile and flexible concept for microfabrication of complex MOFs patterns on large surfaces. Our method relies on the engineering of easily-writable sheets of precursor metal oxide nanoparticles that are loosely bonded to a supporting substrate and can be removed by low-power laser ablation, resulting in well-defined in-depth MOFs patterns. The gas-phase conversion of these patterned ceramic nanoparticle sheets results in monolithic MOFs objects with arbitrarily shaped geometries and thickness of up to hundreds of micrometers. We demonstrate the writing of complex patterns of Zeolitic Imidazolate Framework-8 (ZIF-8) by a variety of approaches including ion beam, laser and handheld writing with a pen. Sub-100 nm patterns were achieved by focused ion beam (FIB) among others. Artless handwritings were obtained by using a pen in a similar fashion to writing on a paper. The pure ZIF-8 composition of the resulting patterns is confirmed by a series of physical and chemical characterization techniques, with a small laser-affected area near the patterned edge. This facile MOF precursor-writing approach provides novel opportunities for the design of MOF-based devices with applications ranging from micro-fluidics to renewable energy systems.

Keywords: nanoparticle precursor sheet, writable, metal-organic frameworks, monolithic patterning, high-aspect ratio

1. Introduction

Metal-organic frameworks (MOFs) have high accessible surface areas of typically 1000 to 7000 m^2/g,[1] designable pore chemistry,[2] unique topologies[3] and unsaturated metal nodes,[4] which make them promising for numerous applications such as natural gas upgrading,[5] sensing,[6] catalysis,[7] molecular sieving[8] and integrated electronic devices.[9] The structural engineering of MOFs has attracted great research attention in the last decade, with focused efforts on controlling the size, distribution and shape of continuous MOFs films.

In 2005, using self-assembled organic monolayers (SAMs) in combination with soft lithography, Hermes and co-workers[10] demonstrated the selective growth of thin MOFs films (e.g. MOF-5) on Au(111). In 2009, Ameloot et al.[11] achieved artless MOFs patterns via an electrochemical approach. In 2012, Reboul et al.[12] reported the successful preparation of 3D hierarchical porous MIL-53 and MIL-100 by the pseudomorphic replication. Later in 2015, Stassen et al.[13] reported a CVD-MOF approach enabling the lift-off patterning of thin ZIF-8 films with a maximal thickness of ca. 124 nm and their integration into electronic devices. Building on these achievements various strategies[14] have been proposed to enable more sophisticated MOFs patterns, including direct patterning of oriented MOFs by controlled crystallization from solution,[15] liquid-phase epitaxy (LPE) on top of modified substrates (i.e. Au) using a spray method,[16] patterning of single crystal MOFs,[17] photolithography and microcontact printing of MOFs,[9] top-down MOFs patterning using deep X-Ray lithography,[18] inkjet-print of MOFs (e.g. HKUST-1),[19] directed MOFs growth via micro-confined interfacial synthesis,[20] and electrochemically-assisted microwave deposition of patterned MOFs.[21] More recently, Hirai et al.[22] reported a two-step MOFs patterning approach including the casting of mixed solution with metal ions and ligand on substrates (e.g. glasses) followed by the exposure of such solution precursor under infrared laser irradiation at particular positions. In 2018, Huang and co-workers[8] demonstrated the patterning of ultrathin UiO-66 films via in-situ growth on a

patterned ceramic substrate/precursor. In 2019, Young and co-workers[7] demonstrated the direct manual ink writing of the UiO-66 polymer composites. Stassin et al.[23] successfully deposited the patterned CuCDC and CuBDC MOF thin films on Si and glass substrates via the MOF-CVD approach. In late 2020, Tu et al.[24] reported the irradiation-induced (e.g. X-Ray and electron beam) solubility switch of halogenated ZIFs thus enabling the resist-free high-resolution (e.g. resolution down to sub-50-nm) patterning of MOFs by X-Ray and electron beam lithography. Despite these progresses,[14b, 20, 25] a technique enabling the precise and facile fabrication of micrometer/millimeter-scale deep MOF patterning is lacking. More in details, the limited attainable thickness,[6b, 8-9, 13, 18-19, 23] lack of morphological control[7, 10-11, 15-17, 21-22, 25a] as well as the time-consuming processing steps[8, 18-20, 25b] remain standing challenges for the fabrication of various functional MOFs patterns.

Here, we demonstrate a facile, mask-less approach for design of monolithic MOFs patterns with microscale depth and arbitrary two-dimensional features via direct laser writing on ultraporous nanoparticle networks, used as paper-like ceramic sheet precursors. Loosely bonded metal oxide nanoparticle layers, with tuneable thickness from few nanometres to several micrometres, are fabricated on large surfaces (> 4 cm^2) by scalable cluster-cluster agglomeration of nanoparticle aerosols. In-depth patterns are obtained by facile removal of nanoparticle regions using low power laser ablation. Upon gas-phase reaction with ligands, the nanoparticle precursor sheets are converted into monolithic MOFs patterns with up to sub-millimetre thickness. Diverse monolithic ZIF-8 designs, including capital letters, circular disk arrays, interconnected “impounding reservoir”, geometric drawings, superimposed “zig-zag”, perpendicular and serpentine channels are demonstrated on surface of several centimetre squares with tuneable aspect ratios. The purity and crystallinity of the resulting MOFs patterns was confirmed by a set of complementary physical and chemical characterization approaches including scanning electron microscopy (SEM), transmission electron microscopy (TEM), X-

Ray diffraction (XRD), Fourier-transform infrared spectroscopy (FTIR) and X-ray photoelectron spectroscopy (XPS) mapping. The capability of rapidly fabricating precise microscale MOFs patterns on large surfaces makes this precursor nanoparticle network approach promising for the integration of pre-designed MOF-based devices in numerous applications ranging from micro-fluidic systems[26] to renewable energy systems.[27]

2. Writable Precursor Nanoparticle Sheets

Easily writable ceramic precursor sheets were prepared via three-dimensional self-assembly of metal oxide nanoparticles from scalable flame-made hot aerosols (**Figure 1a**, Supplementary Information Figure S1).[28] Following the cluster-cluster aggregation mechanism in the diffusion-limited regime, the resulting ceramic precursor layers consist of a highly-fragile morphology of metal oxide nanoparticles loosely bonded by van der Waals forces and a porosity of ca. 98%[28a, 29] (Supplementary Information Figure S2a). A small ZnO average particle size of less than 20 nm (Supplementary Information Figure S3) was synthesized to facilitate the full reaction of the ZnO nanoparticles to ZIF-8 via gas-phase conversion.[13, 30]

The thickness of the ZnO precursor sheet was controlled by the aerosol deposition time and arbitrarily fixed to 68 μm to explore the conversion of relatively thick nanoparticle layers into thick high-aspect ratio MOFs patterns (Supplementary Figure S2). The thickness of this precursor nanoparticle layer, and thus resulting MOF films, can be tuned in the 80 nm to 230 μm range via controlling the nanoparticle aerosol self-assembly time (Figure S4).[31] Importantly, while we have focused on the ZnO to ZIF-8 system as a conceptual proof of our patterning approach, the flame synthesis route affords the preparation of a large range of metal oxide nanoparticles aerosols, including CuO and Fe_2O_3, that could be used as precursors for HKUST-1 and MIL-53(Fe), respectively.[31] To be noted, these loosely bonded nanoparticle networks, hold together by weak van der Waals forces, enables facile patterning from the nano-

up to the centimetre-scale by a variety of approaches including ion beam, laser and handheld writing with a pen. Artless handwritings were also obtained by using a pen in a similar fashion to writing on a paper (**Figure 1c-e** and Supplementary Figure S5). Furthermore, an intricate "Rose" (**Figure 1f-j**) approaching sub-100 nm resolution was demonstrated by focused ion beam (FIB) among others.

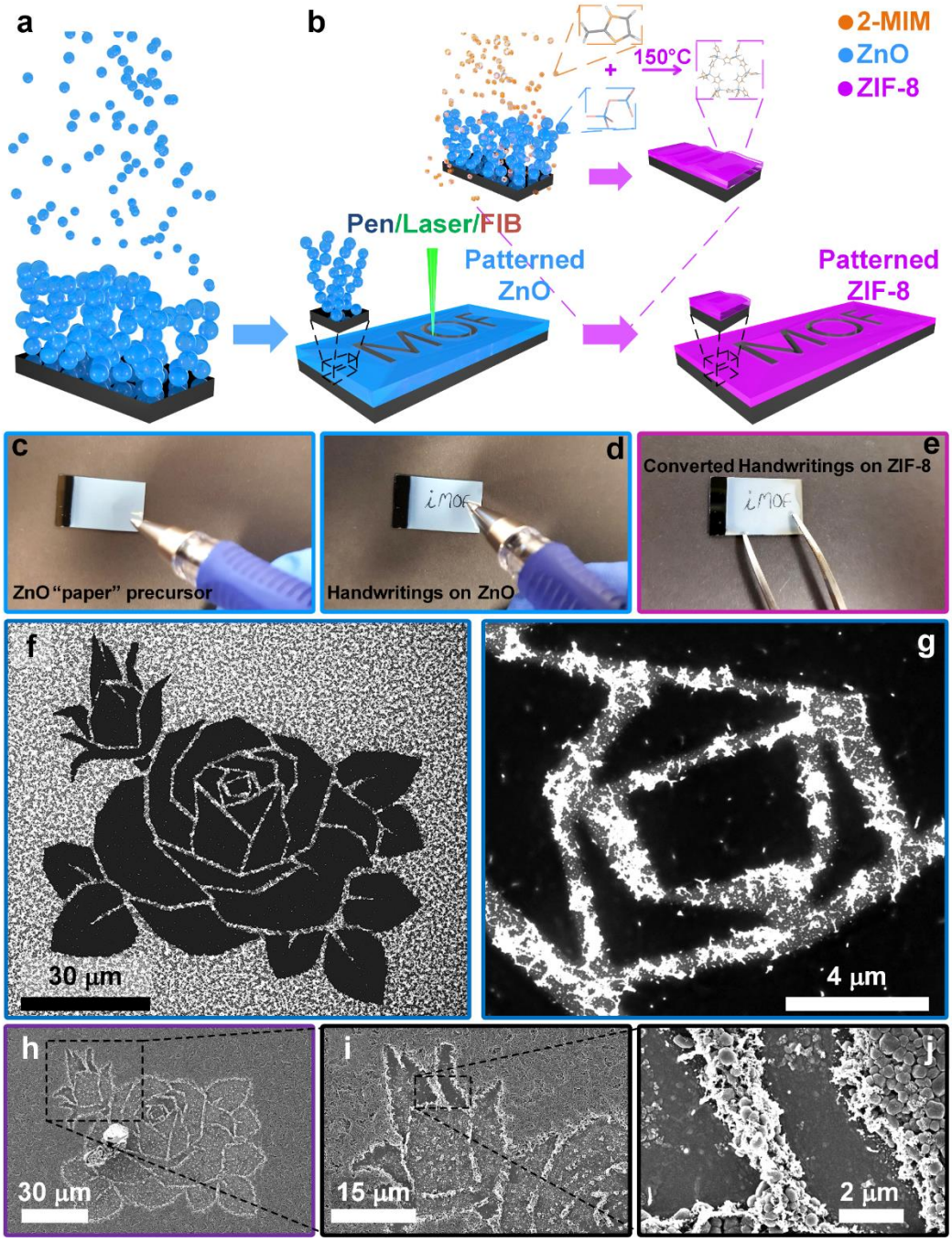

Figure 1 Schematic illustrations. a) Three-dimensional self-assembly of a ZnO nanoparticle precursor sheet from aerosols. b) Rapid in-depth patterning of the precursor nanoparticle sheets

by laser ablation and fabrication of patterned ZIF-8 monolithic films by vapour-phase conversion of the patterned precursor sheets via supply of ligand (2-MIM) vapour. The localized nature of the in-situ gas-phase MOFs conversion result in the precise transfer of the precursor patterns to the MOFs film. c) A ZnO "paper" precursor. d) A phrase "iMOF" is written on the ZnO "paper" precursor. e) The pattern "iMOF" remains in the converted MOF film. f) SEM image of a "rose" drawn on ZnO nanoparticle precursor sheet using FIB. g) High magnification SEM image of the central part of the "rose". h) SEM image of the "rose" on the converted ZIF-8 film. i) Enlarged SEM image of the bud in panel (h), top left. j) High magnification SEM image of the part labeled in (i).

The patterning of the ZnO precursor sheets (**Figure 1b**, Supplementary Information Figure S6) was conducted using a computer-assisted programmable micromachining laser ablation system (JPSA IX-100). Thanks to the fragile nature of the nanoparticle precursor layers, upon a short-timed laser irradiation, the exposed layer surface is removed via Coulomb Explosion, in line with the intense electromagnetic fields of the laser.[32] This enabled a rapid deep lithography of the nanoparticle precursor films. Notably, an exemplary set of complex ZnO precursor patterns, having a depth of 68 μm, were obtained within less than 30 s over a geometrical surface of 4 cm^2 (**Figure 2a**). By testing the same laser ablation protocol on dense ZnO films, a maximum thickness of 0.8 μm could be used for the fabrication of patterns; this highlights the important contribution of the porous ZnO nanoparticle network for the fabrication of thick patterns.

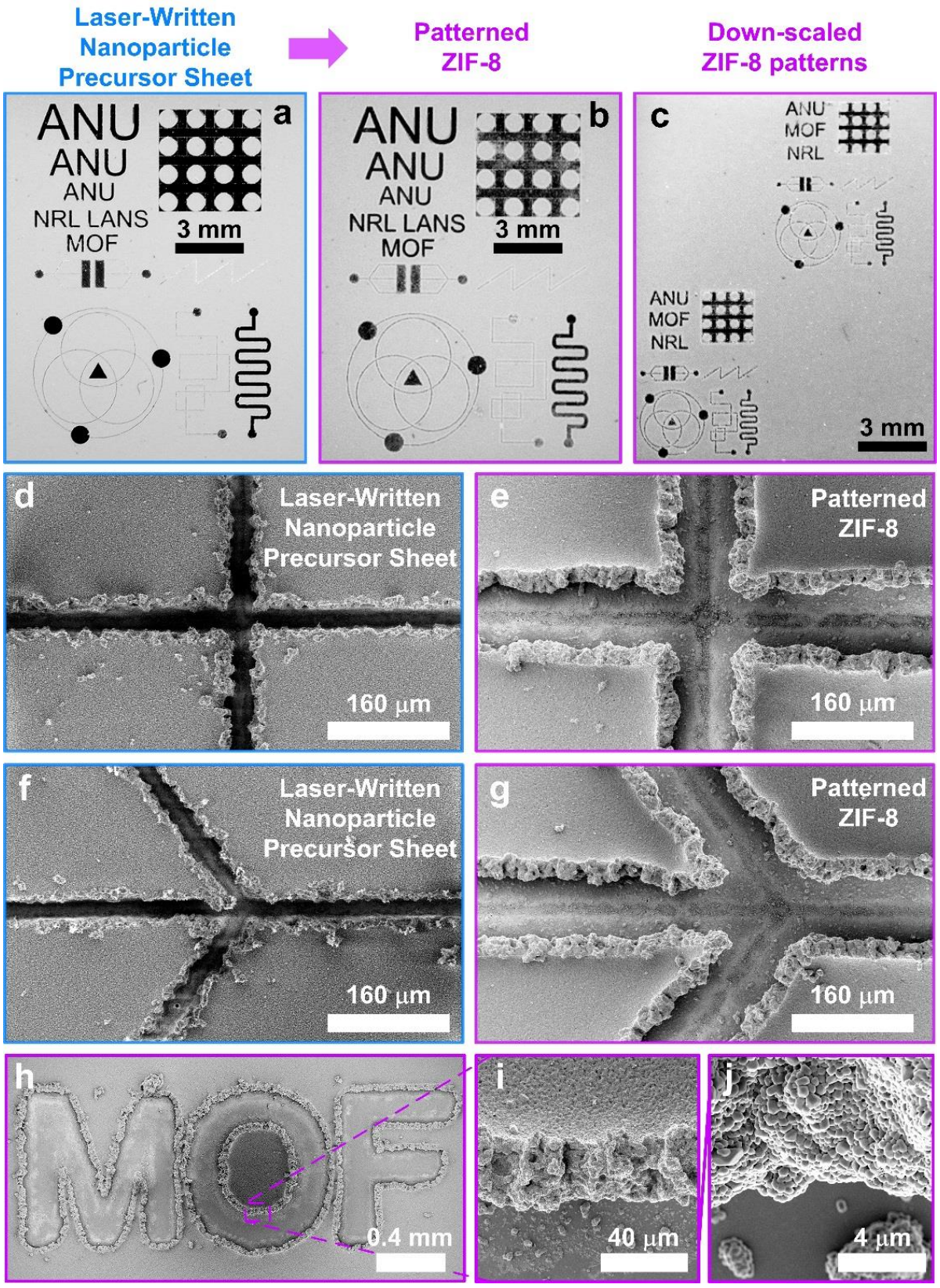

Figure 2 Laser-written nanoparticle precursor sheets and patterned MOF films. a) Optical image of a patterned ZnO precursor sheet. b) Optical image of the resulting patterned ZIF-8 film, obtained by vapour phase conversion of the precursor sheet in (a). c) Optical image of a patterned ZIF-8 with reduced dimension of the original drawings in (a). d) Orthogonal intersecting channels patterned on the ZnO precursor sheet and (e) the same pattern after

conversion to ZIF-8 pattern. f) Arrow-like four-direction pivot patterned on the ZnO precursor sheet and (g) the same pattern after conversion to ZIF-8 pattern. Diverse patterns were laser-written on ZnO precursor films (with a total dimension of ca. 1.9 × 2.0 cm^2 and a reduced total dimension of ca. 0.9 × 1.0 cm^2), including the negative patterns of capital letters (top left in panel a), 4 × 4 array of disks with a designed diameter of 200 μm each (top right in panel a), rectangular "impounding reservoir" connected to a circular "pool" via three channels (middle left in panel a), "zig-zag" channel (middle right in panel a), drawings of geometric figures (bottom left in panel a), perpendicular channels (bottom middle in panel a) and a serpentine channel (bottom right in panel a). h) A ZIF-8 film patterned with "MOF" (Figure 2b top left). i-j) Higher magnification SEM images of the labelled edge in (h). Colour codes: blue for patterned ZnO, violet for pattern ZIF-8.

The laser processing speed and loop numbers (Supplementary Information Laser parameters and descriptions of different patterns) were adjusted to the required amount of ZnO to be removed for each pattern and the required resolution, while keeping a constant laser fluence of ca. 0.18 J/cm^2. For instances, low resolution patterns such as capital letter (**Figure 1b, 2a**) were written at the relatively high processing speed of 15 mm/s in 5 processing loops. However, when a higher resolution is required (i.e. all the other patterns having different geometrical shapes) the laser writing speed was set at 5 mm/s. In **Figure 2a**, lines were obtained within 4 writing loops, while the disk arrays were written with 10 loops because of both contribution 1) the curvature required for the disks and 2) the larger amount of ZnO to be removed. The number of loops was increased to 15 for the circles, triangles and rectangles following the increasing amount of ZnO to be removed. Overall, these fragile nanoparticle precursor sheets provide an easily laser-writable material for the rapid fabrication of deep ceramic patterns with standard micro-machining laser systems without the need for laborious infrastructure requirements such as those for removal of heat generated by high power laser ablation of dense ceramic films.[33]

Comparing to conventional compact thin film precursors, made of dense ceramic layers, the energy required to pattern our nanoparticle network precursor sheets is much lower. In more details, given the identical laser settings (e.g., input power, beam size, wavelength, current etc.) and geometry design, we were able to achieve 68 μm deep patterns in the ZnO nanoparticle

network precursor, while dense ZnO films (i.e., sputtered ZnO thin film), we could only pattern 800 nm depth. This allows for the facile and rapid mask-less patterning of very thick (μm-mm) MOF layers that are required for various applications, such as microfluidic channels and enzymatic reactors.

3. High-Fidelity Conversion of Patterned MOFs Monoliths

Monolithic MOFs films with high aspect-ratio patterns were obtained by vapour-phase conversion[13, 31]of the laser-ablated precursor sheets (**Figure 1b**). **Figure 2b** shows a patterned ZIF-8 film with a surface of 4 cm^2 obtained by exposure of the ZnO precursor sheet to 2-MIM vapour at 150 °C. Notably, the cross-sectional SEM images of the pattern MOF film in **Figure 2** (Supplementary Information Figure S2b) indicates that a patterned monolithic MOF film is obtained. The ZIF-8 pattern dimensions could be easily scaled down by four times to a total surface of ca. 1 cm^2 without major loss of resolution (resolution of ca. 70 μm or less) (**Figure 2c**). Notably, the resolution is mainly determined by the parameters (e.g. dimensions, output power and wavelength) of the accessible light source, advanced lithography technique such as X-Ray and electron beam would drastically enhance the resolution possibly down to nanometre-scale.[24]

Figure 2d shows two orthogonally intersecting channels with a width of 24 μm written on the ZnO precursor sheet. Upon conversion to ZIF-8 (**Figure 2e**), the patterned design was preserved and a broadening of the channels could be observed, resulting in two intersecting 70 μm wide channels surrounded by a monolithic ZIF-8 film. Such channel broadening could only be observed for laser patterning at relatively large-scale (i.e. micrometer scale in width). This might attribute to the localized sintering of few ZnO nanoparticles during laser processing. After gas phase MOF reaction, the shrinkage and densification of those regional networks consisting of sintered ZnO nanoparticles/clusters located at the patterned edges would result

the broadening of channels. Notably, the channel broadening effect becomes muted for nanoscale patterning thanks to the accurately-confined energy dispersion of FIB. **Figure 2f** shows two arrow-like intersecting channels written on the ZnO sheet with the same laser spot size of 24 μm, and resulting in the same 70 μm width intersections on ZIF-8 films. Importantly, all precursor pattern features, such as the sharp acute-angular (52°) back-walls and obtuse-angular (128°) front-walls (**Figure 2f-g**), were well-retained without fracturing of the resulting monolithic ZIF-8 film. The precise transfer of the original ceramic nanoparticle pattern to the MOFs is attributed to the localized reaction of the precursor nanoparticles with the 2-MIM ligand vapour.

The dense packing of the resulting ZIF-8 film grains was confirmed by morphological analysis over large regions of the film surface. **Figure 2h-j** shows higher magnification SEM characterization of a negative pattern of capital letters "MOF" within a ZIF-8 film. Notably, a dense and homogenous film morphology is observed throughout the bulk, patterned area and interface. The ZIF-8 grains reveal a uniform size distribution with a visible grain size of ca. 400 – 550 nm. A sharp deep interface is observed at the pattern border with micrometre range roughness giving a highlighted appearance to the patterned area (**Figure 2h**). Few MOF grains are sitting within 30 μm of the pattern wall on the substrate surface (**Figure 2h-j**), which are attributed to those ZnO nanoparticles sticking to the substrate surface during the conversion of the dense ZIF-8 film.

To demonstrate the ease of obtaining increasingly more sophisticated MOFs pattern designs, various structures were written on the precursor sheets (**Figure 2a**) with arbitrarily tuneable dimensions (e.g. 4 cm^2 and 1 cm^2), and transferred into monolithic ZIF-8 films patterns. The latter designs included the negative patterns of capital letters (**Figure 2c**, top left), 4 × 4 array of disks with a diameter of 200 μm and 100 μm (**Figure 2b-c**, top right), rectangular

impounding reservoir connected to a circular pool via three channels (**Figure 2b**, middle left), zig-zag channel (**Figure 2b**, middle right), intersecting circles with full and empty surfaces as well as triangles (**Figure 2b**, bottom left), long perpendicular intersecting channels (**Figure 2b**, bottom middle) as well as a serpentine channel (**Figure 2b**, bottom right). These experiments demonstrate the potential of the laser ablation protocol for the fabrication of thick patterns of pure ZIF-8 MOFs with pre-determined shapes.

Figure 3 shows higher magnification of the 24 μm deep rectangular "impounding reservoir" (**Figure 3a-c**) connected to three horizontal channels (70 μm wide), the circular pool of 480 μm in diameter connected to the serpentine channel (370 μm wide) (**Figure 3d-f**,) and the curved channel (70 μm wide) written under a triangle (**Figure 3g-i**). The higher magnification edge-surface views of the above pattern borders (**Figure 2i-j**, **Figure 3 b-c**, **e-f** and **h-i**) show no visible compositional difference from the bulk film surface, indicating that the laser-ablation writing of the ZnO nanoparticle precursor sheets has negligible impact on the MOFs conversion process. The latter designs show feasibilities for the rapid patterning of deep (i.e. 24 μm) and complex curved MOFs structures with micro-scale precision on surfaces of several centimetre squares.

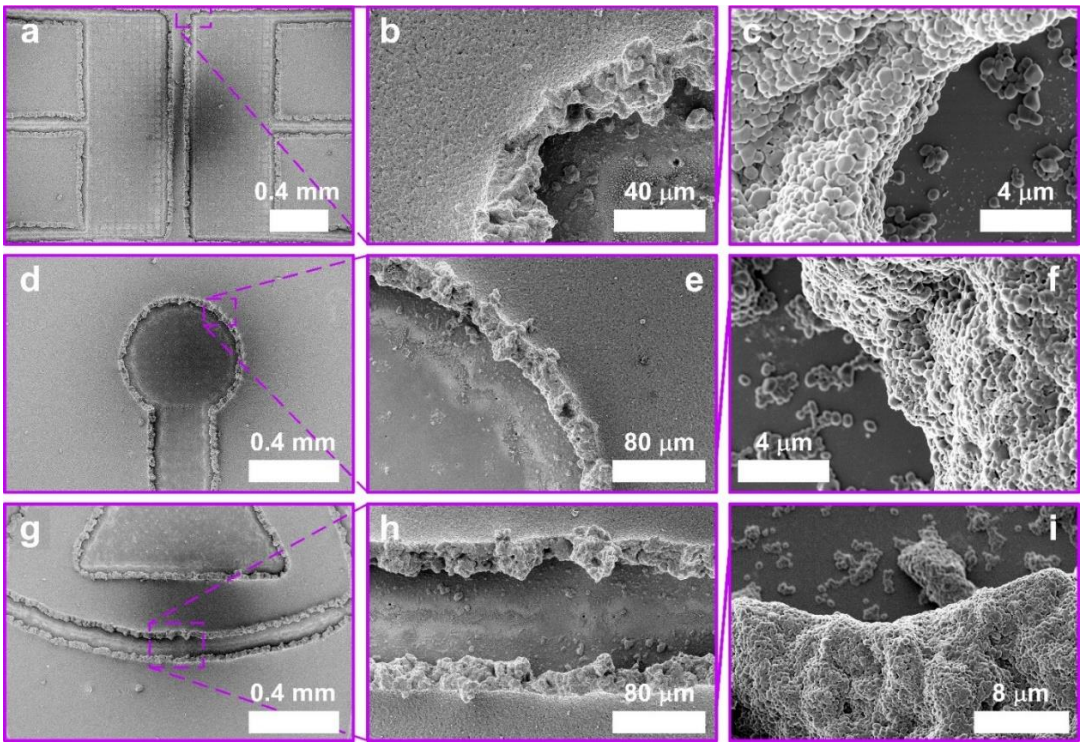

Figure 3 Magnifications of patterned ZIF-8 monolithic films. a) A patterned rectangular "impounding reservoir" connected to three channels (Figure 2b middle left). b-c) Higher magnification SEM images of the labelled corner in (a). d) A circular "pool" connected to a serpentine channel (Figure 2b bottom right). e-f) Higher magnification SEM images of the labelled edge in (d). g) A curved channel under a triangle (Figure 2b bottom left central). h-i) Higher magnification SEM images of the labelled channel walls in (g).

To investigate the mechanical stability of our patterned MOF layers, standard abrasion test (ASTM D5264 - 98) was adopted for over 1600 cycles with 2.27 kg loading. Figure S7 the thickness, measured by confocal microscopy, of a representative ZIF-8 layer with an initial thickness of ca. 8.5 ± 0.90 μm before and after the abrasion cycles. After the first 800 cycles, the initial layer thickness is reduced from ca. 8.5 ± 0.90 μm to ca. 5.5 ± 0.63 μm. This might attribute to removal of a top layer, consisting of more loosely ZIF-8 particles converted from redeposited ZnO nanoparticle clusters during laser processing. Further abrasion test of up to 1600 cycles reveals a nearly unvaried thickness, showing that our patterned MOF are sufficiently robust for handling and possible utilization in microfluidic devices.

The complete conversion of the ceramic precursor sheet into a MOF film was confirmed by a complementary set of chemical and physical characterization approaches including XRD, FTIR, XPS, HRTEM and HAADF-STEM with elemental mappings, aiming at identifying possible contamination arising from the laser-ablation process (**Figure 4a-b)**. The XRD analysis were carried out on the bare Si wafer used as substrate, pure flame-made ZnO powders, patterned (flame-made) ZnO precursor sheet on the Si wafer substrate, resulting patterned ZIF-8 monolithic film on the Si wafer substrate, and representative ZIF-8 crystals synthesized via an alternate aqueous system synthesis route.[34] The XRD characteristic peaks of the ZnO precursor sheet (**Figure 4c**, light blue line) reveal a wurtzite ZnO crystal structure that is in line with the diffraction patterns of the ZnO nanoparticles (**Figure 4c**, dark blue line) collected from the flame-made aerosols with glass fibre filters. After reaction with the 2-MIM vapour, the ZnO wurtzite diffraction peaks of the precursor sheet were substituted by the diffraction peaks of the sodalite (**sod**) ZIF-8 crystal structure (**Figure 4c**, violet line). The latter matched well with those of the ZIF-8 crystals (**Figure 4c**, orange line), synthesized via the aqueous system route.[34] To further confirm the conversion of the patterned ZnO precursor sheet to ZIF-8, FTIR measurements were conducted on the same samples (**Figure 4d**). The characteristic stretching of Zn-O bond[28b] at 440 cm^{-1} was observed for the patterned ZnO precursor sheet (**Figure 4d**, light blue line), in line with that of the ZnO powders (**Figure 4d**, dark blue line). Upon reaction with the 2-MIM vapour, the characteristic Zn-O bond of the ZnO was replaced by the characteristic Zn-N bond[13] of ZIF-8 at 423 cm^{-1} (**Figure 4d**, violet line). Furthermore, the characteristic modes of ZIF-8 imidazole ring observed at 1500 – 1350, 1350 – 900 and 800 – 600 cm^{-1} (**Figure 4d**, violet line) were assigned to the ring stretching, in plane bending, and out of plane bending vibrational modes, respectively. All the FTIR modes were also in good agreement with those observed with the ZIF-8 powders **(Figure 4d**, orange line), obtained via

solution-based synthesis.[34] The combined XRD and FTIR analyses suggest a complete conversion of the ZnO ceramic precursor to **sod** ZIF-8.

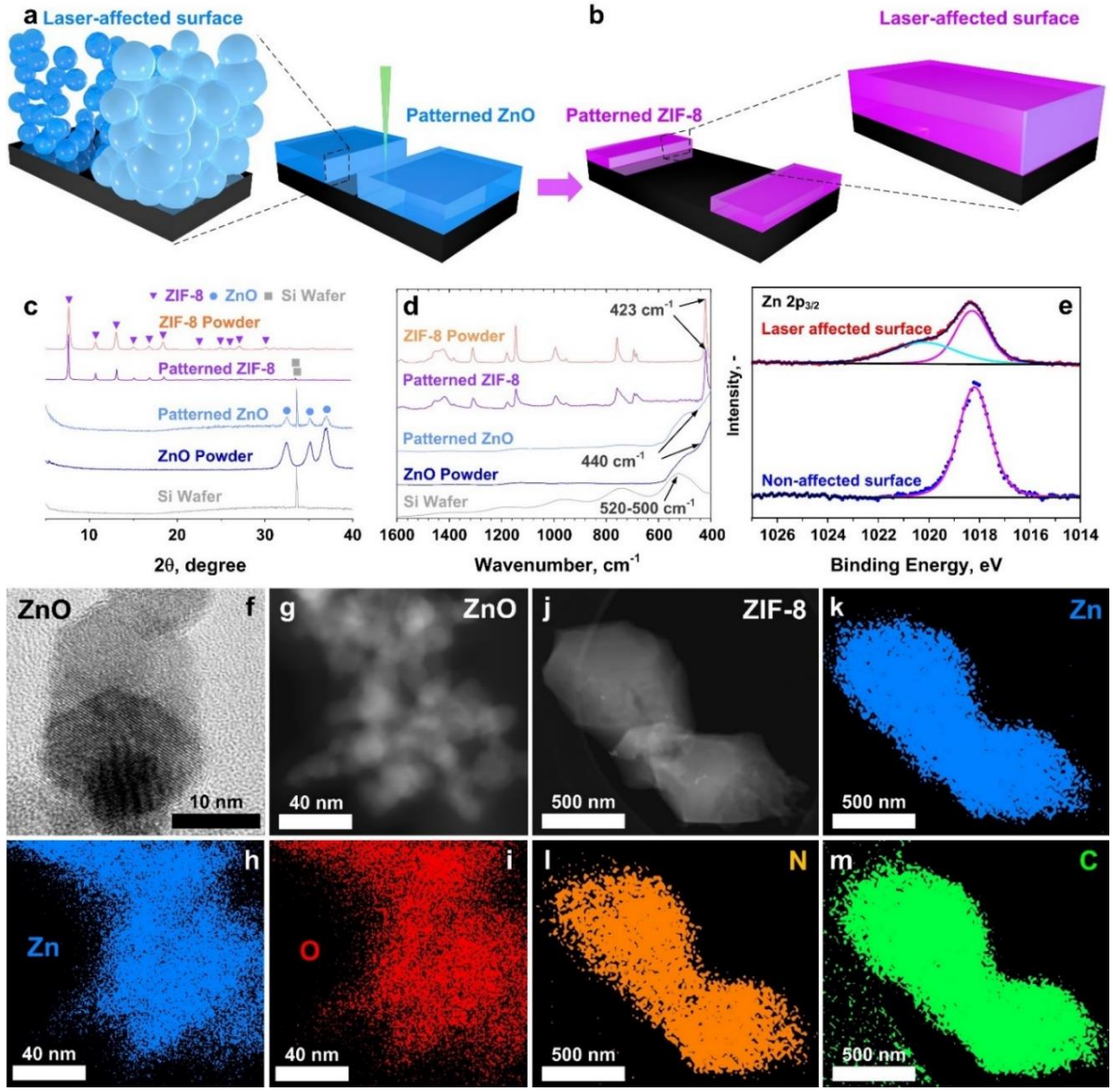

Figure 4 Pattern composition. a) Schematic representations of the laser-affected surfaces on the ZnO precursor sheet and (b) after gas-phase conversion to ZIF-8. Colour codes for (a) & (b): ZnO (transparent dark blue), ZIF-8 (transparent violet), laser-affected surfaces (semi-transparent light blue). c) XRD of the bare Si wafer substrate (light grey line), flame-made ZnO nanoparticle powders (dark blue line), patterned (flame-made) ZnO precursor film on top of a Si wafter substrate (light blue line), resulting patterned ZIF-8 film on top of a Si wafer substrate (violet line), and ZIF-8 powders synthesized via an established aqueous system route (orange line). d) FTIR of the bare Si wafer substrate (light grey line), flame-made ZnO nanoparticle powders (dark blue line), patterned (flame-made) ZnO precursor film on top of a Si wafter substrate (light blue line), resulting patterned ZIF-8 film on top of a Si wafer substrate (violet line), and ZIF-8 powders synthesized via an established aqueous system route (orange line). e) Zn $2p_{3/2}$ high resolution XPS point measurements of the laser-affected edge-surface of a converted ZIF-8 pattern (red dots with black line) as well as the unaffected fully converted ZIF-

8 surface (blue dot with purple line). f) HRTEM of ZnO nanoparticles detached from patterned ZnO nanoparticle network precursor. g) HAADF-STEM of ZnO nanoparticles detached from patterned ZnO nanoparticle network precursor. h-i) Elemental mappings of Zn and O for the detached ZnO nanoparticles from ZnO nanoparticle network precursor. Colour codes: Zn, blue; O, red. j) HAADF-STEM of ZIF-8 particles detached from patterned monolithic ZIF-8 film. k-m) Elemental mappings of Zn, N and C for ZIF-8 particles detached from patterned monolithic ZIF-8 film. Colour codes:Zn, blue; N, orange; C, green.

To further investigate the possible presence of minor impurities, XPS and TEM analysis were pursued. Two representative locations were determined for XPS point measurements on both the patterned ZnO precursor sheets and resulting ZIF-8 monolithic films (Supplementary Information Figure S8a). The latter consisted of a location sitting exactly on the edge of a patterned disk (Supplementary Information Figure S8a, red point, location-**i)** and a location few hundred micrometres distant from the pattern border (Supplementary Information Figure S8a, blue point, location-**ii**).

High-resolution Zn core level spectra before conversion at the pattern edge (Supplementary Information Figure S8) indicated a pure ZnO surface chemistry (Supplementary Information Figure S8b) with a binding energy of 1021 eV and 1044 eV for Zn^{2+} $2p_{3/2}$ and Zn^{2+} $2p_{1/2}$, respectively. While after conversion a mixed surface chemistry (Supplementary Information Figure S8c) was observed which is attributable to a major ZIF-8 component with some ZnO contribution after conversion. To clarify, the Zn^{2+} $2p_{3/2}$ spectra (**Figure 4e**, black line with red dots) of the laser-ablated surface (Supplementary Information Figure S8a, red point, location-**i**) after conversion can be fitted by two quasi-Gaussian components (**Figure 4e**, blue and purple line) peaking at 1018 and 1021 eV corresponding to the low energy Zn-N covalent bonding and higher energy Zn-O ionic bonding, respectively, indicating a mixed surface chemistry consisting of both ZIF-8 and ZnO residuals. In stark contrast, the Zn^{2+} $2p_{3/2}$ spectra of the location distant from the pattern edge (**Figure 4e**, violet line with blue dots at the bottom) after conversion presented a pure ZIF-8 surface chemistry with a single component peaking at 1018

eV reflecting the covalent Zn-N bonding only, indicating the complete replacement of Zn-O ionic bonding by Zn-N covalent bonding.

HRTEM, HAADF-STEM and elemental mappings were conducted on ZnO nanoparticles (**Figure 4f-i**) and ZIF-8 grains (**Figure 4j-m**) detached from the patterned ZnO precursor sheets and ZIF-8 films, respectively. The former revealed a pure ZnO nanoparticle composition (**Figure 4f-g**) with a uniform distribution of Zn (**Figure 4h**) and O (**Figure 4i**). The latter grains revealed a pure ZIF-8 grain composition (**Figure 4j**) with a uniform distribution of Zn (**Figure 4k**), N (**Figure 4l**) and C (**Figure 4m**) and without any observation of oxygen containing ZnO domains. The combined XPS and electron microscopy analysis indicates the conversion of the ZnO precursor into ZIF-8 with the presence of a small fractional content of ZnO impurities localized at the pattern edge. The latter is possibly attributed to the sintering of the ZnO nanoparticles at the laser-exposed pattern edge. The extreme local temperature induced by laser[32, 35] may result in the sintering growth and packing of the ZnO nanoparticles (**Figure 4a**). Particles growing above 20 nm and packed clusters with porosity less than 95%[31] may experience only partial conversion to ZIF-8 structures by gas phase conversion, due to the ligand reaction being limited within the first 10 nm of the particle surface.[13, 30] Due to the drastic reduction of laser energy within thin films,[35] the sintered area would possibly occur within a maximal penetration radius of ca. 100-112 nm[35] from the laser-ablated area. Overall, given the limited fabrication methods of monolithic MOFs,[13, 23, 30, 36] the feasibility of rapidly fabricating arbitrarily-designed MOFs patterns with micrometre scale thickness has various potential applications including micro-fluidic[26] and renewable energy systems.[27]

4. MOFs patterns of micrometre-scale depth with a broad resolution range down to sub-100 nm

To further demonstrate the resolution range and flexibility of our approach, we performed further mask-less patterning of our ZnO nanoparticle sheets by high-resolution focused ion

beam (FIB) and with a low-resolution hand-held pen. We demonstrate that our approach allows for paper-like writing/patterning of MOFs with any arbitrarily geometry. **Figure 1c-d** show the writing of "iMOF" by smooth and fluid strokes on our ZnO nanoparticle precursor sheets. After conversion, the "iMOF" pattern is well preserved with no loss of details (**Figure 1e**). This facile mask-less patterning procedure has potential for the rapid patterning of very large MOF surfaces that do not require high resolutions including microfluidics,[26c, 37] biosensors[26a] and enzymatic reactors.[38]

To demonstrate high resolution patterning with our approach, a "Rose" with a total dimension of ca. 90 × 60 μm^2 was patterned on the ZnO nanoparticle precursor sheet (**Figure 1f-g**) by FIB. Notably, this is an intricate pattern with tiny line width of less than 270 nm (**Figure 1g**). After gas phase reaction, no distortion could be found on the patterned ZIF-8 layer (**Figure 1h-j**) and the total dimension of the "Rose" remains unchanged with no loss of original details. For the very tiny line of less than 300 nm in width drawn on the ZnO precursor sheet (**Figure 1g**), a slight increase of line width can be observed (i.e., **Figure 1h-j**, the resulting ZIF-8 is ca. 400 nm). This is attributed to the expansion of the lattice structure from ZnO to ZIF-8. In details, our nanoparticle precursor sheets consist of ZnO nanoparticles with an average diameter of ca. 14.8 nm, thus, the size of resulting ZIF-8 particles should be around 250 nm, considering a 17-fold lattice expansion. This is rarely achieved among the most up-to-date advanced MOF pattering techniques,[7-8, 21-24] and has never been achieved with deep MOF patterns of tens of micrometers. In light of these results, our patterning method present a very high-resolution that is likely to be sufficient to most envisioned MOF applications.

With respect to the broader applicability of our method, it is important to note that our proposed approach is compatible with the broad family of CVD-generated MOFs.[13, 23-24, 31] As the flame aerosol synthesis approach, utilized here, is capable to synthesize a large family of metal oxides,[39] which makes it an ideal tool for synthesizing nanoparticle precursor sheets for

various MOFs. To demonstrate this concept, we have now converted MIL-53 (Figure S10-11) and HKUST-1 films (Figure S12-13) from Fe_2O_3 and CuO nanoparticle network precursor sheets, respectively. XRD results of both Fe_2O_3 (Figure S11) and CuO (Figure S13) precursor sheets before and after conversion reveals the successful production of other MOF families rather than ZIFs via our proposed method. This further indicates the applicability of our proposed patterning procedure across various MOF materials.

To summarize, our method enables (i) both low and high-resolution patterning down to ca. 100 nm, (ii) is applicable to various MOF families and highly compatible with existing CVD-MOF growth, and (iii) afford in-depth monolithic MOFs patterns of up to several tens of micrometers in thickness.

5. Conclusion

In summary, we have demonstrated the facile fabrication of centimetre-scale monolithic MOFs patterns with depth of tens of micrometres and a broad range of resolution via various approaches including FIB, laser ablation and handheld pen. Easily laser-writable nanoparticle sheets, consisting of loosely connected nanoparticle networks of less than 20 nm in diameter and a porosity of 98%, were introduced as a large-area precursor for the design and fabrication of deep and arbitrarily complex MOFs patterns. Gas-phase conversion of patterned ZnO nanoparticle sheets, resulted in monolithic MOFs films, with designable dimensions and thickness over surfaces of several square centimetres. A range of representative ZIF-8 patterns were demonstrated including 24 μm-deep capital letters, circular disk arrays, interconnected impounding reservoir, geometric drawings, superimposed zig-zag, perpendicular and serpentine channels. Notably, Artless handwritings were also patterned on ZIF-8 film using a handheld pen. A vastly pure MOF composition of the converted pattern was confirmed by a series of physical and chemical characterizations with a small fractional content of ceramic impurity localized at the laser-ablated pattern edge. We believe that this nanoparticle-precursor

sheet approach provides a promising route for the engineering of functional MOFs patterns and their integration in devices with envisioned applications in microfluidics, energy storage and filtration.

6. Experimental Section

A liquid-fed flame reactor (Supplementary Information Figure S1) was utilized to generate the aerosol source consisting of ZnO nanoparticles with an optimal concentration for the ZnO nanoparticle networks (NN) precursor preparations as reported elsewhere.[28a] In details, a mixed solution of zinc-naphthenate dissolved in m-xylene with a total metal concentration of 0.3 mol L^{-1} was used as the metal precursor for the production of ZnO nanoparticle with an averaged particle size of 14.8 nm (Supplementary Information Figure S3). All ZnO NN precursors were collected at 20 cm height above the burner (HAB) resulting in a sufficiently high porosity of 98%.[28a, 29] The thickness of ZnO NN precursor was arbitrarily kept as 68 μm everywhere. The control ZnO powders were collected at the same HAB.

The laser ablation was carried out using a computer-assisted programmable micromachining system, namely JPSA IX-100, equipped with the PRISMA-532-14-V laser source. The original drawings of various patterns (Supplementary Information Figure S6) were designed via Microsoft Visio, which is a compatible software with the applied micromachining system. After imported to the micromachining operation system, all dimensions were specified based on client requirements (e.g. the total dimensions of 2.0 × 1.9 cm^2 and 1.0 × 0.95 cm^2). Varied laser powers (200 – 300 mV), processing speeds (5 – 15 mm/s) and numbers of processing loops (5 – 10 loops) were customized according to different patterns.

The patterned monolithic ZIF-8 films were prepared via converting those patterned ZnO NN precursors in gas phase. In particular, the patterned ZnO NN precursor together with a glass

vial containing 2-methylimidazole (2-MIM) solid crystals were placed in a Teflon lined stainless steel autoclave. The auto-clave was sealed and heated up to 150 °C with a ramping of 10 °C/min, and reaction was held for 18 hours. The control ZIF-8 powders were synthesized using a modified aqueous system based on previous report.[34] In details, two solutions were prepared separately in advance, including solution-1 of 8 mmol 2-MIM dissolved in 300 mmol water and solution-2 of 1 mmol zinc acetate dissolved in 300 mmol water. Then, solution-2 was added into solution-1 companied with magnetic stirring for 2 hours at room temperature. White powder was collected by centrifugation for 10 min, washing twice with ethanol and drying overnight in the oven (60 °C).

The XRD measurements were conducted using a Bruker system (XRD, D2 Phaser, USA) equipped with Cu Kα radiation of average wavelength 1.54059 Å. The FTIR data were collected using Bruker ALPHA II FTIR Spectrometer with the PLATINUM ATR module from 4000 to 400 cm^{-1}. The XPS point measurements were carried out and collected using a Thermofisher Kratos Axis Supra photoelectron spectrometer, with a monochromated Al kα source (1486.7 eV) at pass energy 20.

The SEM morphological characterizations were conducted using a Zeiss Ultraplus (FESEM) at 3 kV. The HRTEM, HAADF-STEM and elemental mappings were collected using a JEOL 2100F FEGTEM at 200 kV.

Focused Ion Beam (FEI Helios 600 NanoLab) was used for fine pattering of ZIF-8 films (Supplementary Information, Figure S9).

A motorized device (Supplementary Information, **ZIF-8 cloth rub durability test**, Figure S14 and Movie S1) was applied for the cloth rub test.

Supporting Information
Supporting Information is available from the Wiley Online Library or from the author.

Acknowledgments

A.T. gratefully acknowledges the support from Australian Research Council FT170100224, DE160100569, DP190101864, and LP170101157, and the NATO Science for Peace and Security Programme. R.B. gratefully acknowledges the support of National Natural Science Foundation of China (Grant. No. 12102221). R.B. gratefully acknowledges the support of Office of China Postdoc Council (OCPC) and Tsinghua University for the International Postdoctoral Exchange Fellowship Program (Talent-Introduction Program) YJ20200112. R.B. gratefully acknowledges the support of China Postdoctoral Science Foundation for the fellowship (2021M691795). The microscope analysis was conducted in the Centre of Advanced Microscopy (CAM) at ANU node of the Australian Microscopy & Microanalysis Research Facility (AMMRF). The Australian National Fabrication Facility (ANFF) is acknowledged for materials characterizations. Hua Chen and Felipe Kremer are acknowledged for helpful discussions on microscopy imaging. R. B gratefully acknowledges the assistance of the Solar PV Group in RSEEME, ANU, for the laser ablation processing. The PV Group receives significant support from the Australian Renewable Energy Agency. P.F. acknowledges European Research Council under the European Union's Horizon 2020 Program (FP/2014‑2020)/ERC Grant Agreement no. 771834 - POPCRYSTAL

([#]R. Bo and M. Taheri contributed equally to this work)

Received: ((will be filled in by the editorial staff))
Revised: ((will be filled in by the editorial staff))
Published online: ((will be filled in by the editorial staff))

TOC Entry: Rapid and facile patterning of MOFs on the centimeter scale. Diverse patterns with pure and crystalline sodalite (**sod**) ZIF-8 composition have been showcased by low-power laser writing of nanoparticle network sheets, providing some unique beneficial features for the design of scalable and well-defined MOFs geometries for various cross-disciplinary applications.

Keywords: nanoparticle precursor sheet, writable, metal-organic frameworks, monolithic patterning, high aspect ratio

Renheng Bo[1,2,3,#,*], Mahdiar Taheri[4,#], Hongjun Chen[1], Jonathan Bradford[5], Nunzio Motta[5], Sachin Surve,[6] Takuya Tsuzuki[4], Paolo Falcaro[7] and Antonio Tricoli[1,*]

Paper-Like Writable Nanoparticle Network Sheets for Mask-Less MOF Patterning

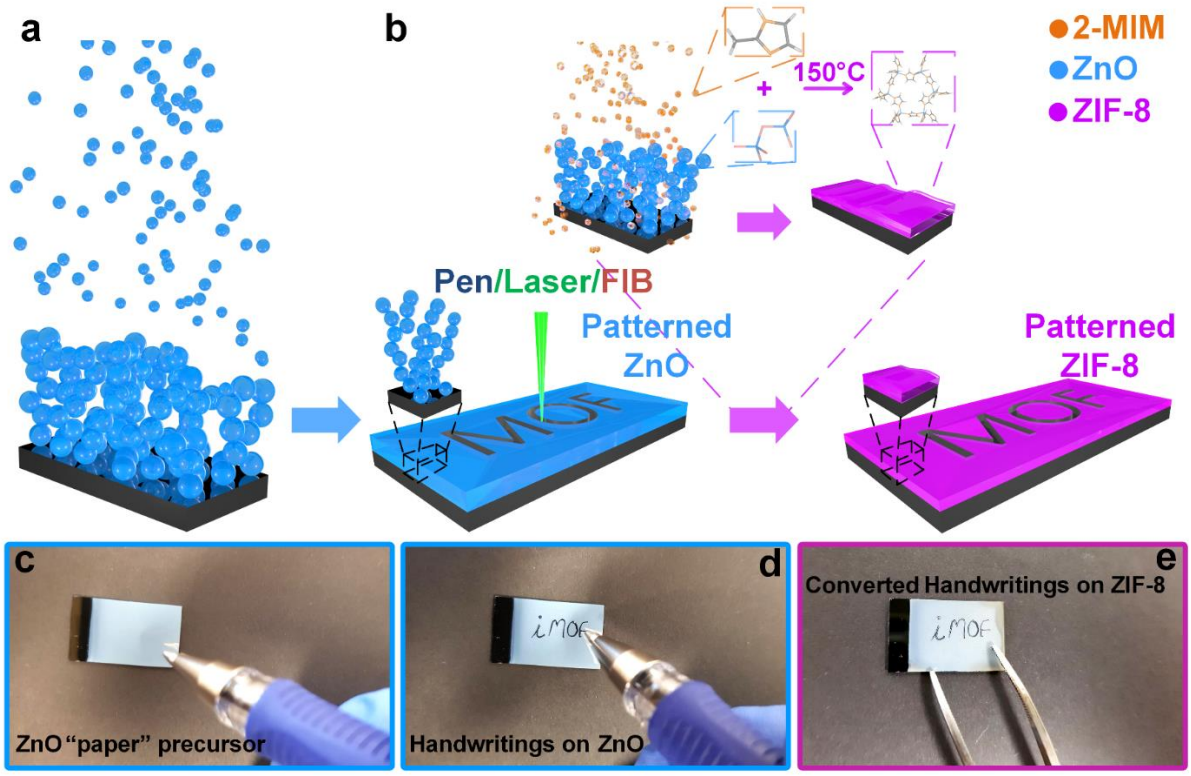

Reference

[1] H. Furukawa, K. E. Cordova, M. O'Keeffe, O. M. Yaghi, *Science* **2013**, 341, 1230444.

[2] a) M. Eddaoudi, J. Kim, N. Rosi, D. Vodak, J. Wachter, M. O'Keeffe, O. M. Yaghi, *Science* **2002**, 295, 469; b) O. M. Yaghi, M. O'Keeffe, N. W. Ockwig, H. K. Chae, M. Eddaoudi, J. Kim, *Nature* **2003**, 423, 705.

[3] N. Stock, S. Biswas, *Chemical Reviews* **2011**, 112, 933.

[4] C. S. Diercks, Y. Liu, K. E. Cordova, O. M. Yaghi, *Nature Materials* **2018**, 17, 301.

[5] Y. Belmabkhout, P. M. Bhatt, K. Adil, R. S. Pillai, A. Cadiau, A. Shkurenko, G. Maurin, G. Liu, W. J. Koros, M. Eddaoudi, *Nature Energy* **2018**, 3, 1059.

[6] a) O. Dalstein, E. Gkaniatsou, C. Sicard, O. Sel, H. Perrot, C. Serre, C. Boissière, M. Faustini, *Angewandte Chemie International Edition* **2017**, 56, 14011; b) M. G. Campbell, S. F. Liu, T. M. Swager, M. Dincă, *Journal of the American Chemical Society* **2015**, 137, 13780.

[7] A. J. Young, R. Guillet-Nicolas, E. S. Marshall, F. Kleitz, A. J. Goodhand, L. B. Glanville, M. R. Reithofer, J. M. Chin, *Chemical Communications* **2019**, 55, 2190.

[8] K. Huang, B. Wang, S. Guo, K. Li, *Angewandte Chemie International Edition* **2018**, 57, 13892.

[9] G. Lu, O. K. Farha, W. Zhang, F. Huo, J. T. Hupp, *Advanced Materials* **2012**, 24, 3970.

[10] S. Hermes, F. Schröder, R. Chelmowski, C. Wöll, R. A. Fischer, *Journal of the American Chemical Society* **2005**, 127, 13744.

[11] R. Ameloot, L. Stappers, J. Fransaer, L. Alaerts, B. F. Sels, D. E. De Vos, *Chemistry of Materials* **2009**, 21, 2580.

[12] J. Reboul, S. Furukawa, N. Horike, M. Tsotsalas, K. Hirai, H. Uehara, M. Kondo, N. Louvain, O. Sakata, S. Kitagawa, *Nature Materials* **2012**, 11, 717.

[13] I. Stassen, M. Styles, G. Grenci, Hans V. Gorp, W. Vanderlinden, Steven D. Feyter, P. Falcaro, D. D. Vos, P. Vereecken, R. Ameloot, *Nature Materials* **2015**, 15, 304.

[14] a) P. Falcaro, D. Buso, A. J. Hill, C. M. Doherty, *Advanced Materials* **2012**, 24, 3153; b) P. Falcaro, R. Ricco, C. M. Doherty, K. Liang, A. J. Hill, M. J. Styles, *Chemical Society Reviews* **2014**, 43, 5513; c) J.-L. Zhuang, A. Terfort, C. Wöll, *Coordination Chemistry Reviews* **2016**, 307, 391.

[15] a) R. Ameloot, E. Gobechiya, H. Uji-i, J. A. Martens, J. Hofkens, L. Alaerts, B. F. Sels, D. E. De Vos, *Advanced Materials* **2010**, 22, 2685; b) S. Li, W. Shi, G. Lu, S. Li, S. C. J. Loo, F. Huo, *Advanced Materials* **2012**, 24, 5954.

[16] H. K. Arslan, O. Shekhah, J. Wohlgemuth, M. Franzreb, R. A. Fischer, C. Wöll, *Advanced Functional Materials* **2011**, 21, 4228.

[17] a) C. Carbonell, I. Imaz, D. Maspoch, *Journal of the American Chemical Society* **2011**, 133, 2144; b) D. Witters, N. Vergauwe, R. Ameloot, S. Vermeir, D. De Vos, R. Puers, B. Sels, J. Lammertyn, *Advanced Materials* **2012**, 24, 1316.

[18] C. Dimitrakakis, B. Marmiroli, H. Amenitsch, L. Malfatti, P. Innocenzi, G. Grenci, L. Vaccari, A. J. Hill, B. P. Ladewig, M. R. Hill, *Chemical Communications* **2012**, 48, 7483.

[19] J. L. Zhuang, D. Ar, X. J. Yu, J. X. Liu, A. Terfort, *Advanced Materials* **2013**, 25, 4631.

[20] J. O. Kim, K. I. Min, H. Noh, D. H. Kim, S. Y. Park, D. P. Kim, *Angewandte Chemie International Edition* **2016**, 55, 7116.

[21] W.-J. Li, J.-F. Feng, Z.-J. Lin, Y.-L. Yang, Y. Yang, X.-S. Wang, S.-Y. Gao, R. Cao, *Chemical Communications* **2016**, 52, 3951.

[22] K. Hirai, K. Sada, *Chemical Communications* **2017**, 53, 5275.

[23] T. Stassin, S. Rodríguez-Hermida, B. Schrode, A. J. Cruz, F. Carraro, D. Kravchenko, V. Creemers, I. Stassen, T. Hauffman, D. De Vos, *Chemical Communications* **2019**, 55, 10056.

[24] M. Tu, B. Xia, D. E. Kravchenko, M. L. Tietze, A. J. Cruz, I. Stassen, T. Hauffman, J. Teyssandier, S. De Feyter, Z. Wang, *Nature Materials* **2021**, 20, 93.

[25] a) S. Wannapaiboon, M. Tu, K. Sumida, K. Khaletskaya, S. Furukawa, S. Kitagawa, R. A. Fischer, *Journal of Materials Chemistry A* **2015**, 3, 23385; b) S. M. Yoon, J. H. Park, B. A. Grzybowski, *Angewandte Chemie International Edition* **2017**, 56, 127.

[26] a) F. Eduati, R. Utharala, D. Madhavan, U. P. Neumann, T. Longerich, T. Cramer, J. Saez-Rodriguez, C. A. Merten, *Nature Communications* **2018**, 9, 2434; b) M. Kaiser, F. Jug, T. Julou, S. Deshpande, T. Pfohl, O. K. Silander, G. Myers, E. Van Nimwegen, *Nature Communications* **2018**, 9, 212; c) J. Li, N. S. Ha, R. M. van Dam, *Nature* **2019**, 572, 507.

[27] a) B. An, Z. Li, Y. Song, J. Zhang, L. Zeng, C. Wang, W. Lin, *Nature Catalysis* **2019**, 2, 709; b) I. Agirrezabal-Telleria, I. Luz, M. A. Ortuño, M. Oregui-Bengoechea, I. Gandarias, N. López, M. A. Lail, M. Soukri, *Nature Communications* **2019**, 10.
[28] a) R. Bo, N. Nasiri, H. Chen, D. Caputo, L. Fu, A. Tricoli, *ACS Applied Materials & Interfaces* **2017**, 9, 2606; b) N. Nasiri, R. Bo, F. Wang, L. Fu, A. Tricoli, *Advanced Materials* **2015**, 27, 4336.
[29] N. Nasiri, R. Bo, H. Chen, T. P. White, L. Fu, A. Tricoli, *Advanced Optical Materials* **2016**, 4, 1787.
[30] S. Tanaka, K. Kida, T. Nagaoka, T. Ota, Y. Miyake, *Chemical Communications* **2013**, 49, 7884.
[31] R. Bo, M. Taheri, B. Liu, R. Ricco, H. Chen, H. Amenitsch, Z. Fusco, T. Tsuzuki, G. Yu, R. Ameloot, *Advanced Science* **2020**, 7, 2002368.
[32]N. Bulgakova, R. Stoian, A. Rosenfeld, I. Hertel, E. Campbell, *Physical Review B* **2004**, 69, 054102.
[33] F. Claeyssens, A. Klini, A. Mourka, C. Fotakis, *Thin Solid Films* **2007**, 515, 8529.
[34] M. Jian, B. Liu, R. Liu, J. Qu, H. Wang, X. Zhang, *RSC Advances* **2015**, 5, 48433.
[35] M. Mansuripur, G. N. Connell, J. W. Goodman, *Applied Optics* **1982**, 21, 1106.
[36] a) P. Falcaro, K. Okada, T. Hara, K. Ikigaki, Y. Tokudome, Aaron W. Thornton, Anita J. Hill, T. Williams, C. Doonan, M. Takahashi, *Nature Materials* **2016**, 16, 342; b) T. Tian, Z. Zeng, D. Vulpe, M. E. Casco, G. Divitini, P. A. Midgley, J. Silvestre-Albero, J.-C. Tan, P. Z. Moghadam, D. Fairen-Jimenez, *Nature Materials* **2017**, 17, 174; c) B. Liu, R. Bo, M. Taheri, I. Di Bernardo, N. Motta, H. Chen, T. Tsuzuki, G. Yu, A. Tricoli, *Nano Letters* **2019**, 19, 4391.
[37] a) B. Okumus, C. J. Baker, J. C. Arias-Castro, G. C. Lai, E. Leoncini, S. Bakshi, S. Luro, D. Landgraf, J. Paulsson, *Nature Protocols* **2018**, 13, 170; b) Y. Yu, L. Shang, J. Guo, J. Wang, Y. Zhao, *Nature Protocols* **2018**, 1.
[38] D. Feng, T.-F. Liu, J. Su, M. Bosch, Z. Wei, W. Wan, D. Yuan, Y.-P. Chen, X. Wang, K. Wang, *Nature Communications* **2015**, 6, 5979.
[39] a) R. Bo, F. Zhang, S. Bu, N. Nasiri, I. Di Bernardo, T. Tran-Phu, A. Shrestha, H. Chen, M. Taheri, S. Qi, *ACS applied materials & interfaces* **2020**, 12, 9589; b) T. Tran-Phu, Z. Fusco, I. Di Bernardo, J. Lipton-Duffin, C. Y. Toe, R. Daiyan, T. Gengenbach, C.-H. Lin, R. Bo, H. T. Nguyen, *Chemistry of Materials* **2021**; c) I. Di Bernardo, J. Bradford, Z. Fusco, J. Mendoza, T. Tran-Phu, R. Bo, N. Motta, A. Tricoli, *Journal of Materials Chemistry C* **2020**, 8, 11896; d) T. Tran‐Phu, H. Chen, R. Bo, I. Di Bernardo, Z. Fusco, A. N. Simonov, A. Tricoli, *Energy Technology* **2019**, 7, 1801052; e) H. Chen, R. Bo, T. Tran‐Phu, G. Liu, A. Tricoli, *ChemPlusChem* **2018**, 83, 569.